J Mater Sci (2009) 44:5852–5860
DOI 10.1007/s10853-009-3826-8

Synthesis and characterizations of nano-sized $Ni(OH)_2$ and $Ni(OH)_2$/poly(vinyl alcohol) nano composite

M. Fathima Parveen · S. Umapathy · V. Dhanalakshmi · R. Anbarasan

Received: 22 April 2009 / Accepted: 20 August 2009 / Published online: 1 September 2009

Abstract Nano-sized $Ni(OH)_2$ was synthesized by a co-precipitation method. Peaks between 500 and 750 cm^{-1} in Fourier transform infrared spectroscopy (FTIR) confirmed the presence of metal hydroxide stretching. Thermo gravimetric analysis inferred that 69 wt% residue remained above 750 °C. High-resolution transmission electron microscopy analysis of $Ni(OH)_2$ revealed its size ranged from 80 to 110 nm with smooth morphology. Scanning electron microscopy inferred that pure $Ni(OH)_2$ has nano rod-like morphology and higher weight percentage of aniline-intercalated $Ni(OH)_2$ has agglomerated structure. UV–Vis spectrum detected the presence of Ni^{2+} ions at 210 nm and the existence of amino group in the basal spacing of $Ni(OH)_2$ was not clearly appeared in the spectrum. Photoluminescence (PL) inferred that aniline-intercalated $Ni(OH)_2$ showed higher PL intensity than the pristine poly(vinyl alcohol) its and nano composite.

M. Fathima Parveen
Department of Physics, Hajee Karutha Rowther Howdia College, Uthamapalayam 625-533, Tamilnadu, India

S. Umapathy
School of Physics, Madurai Kamaraj University, Madurai 625-021, Tamilnadu, India

V. Dhanalakshmi
Department of Polymer Technology, KCET, Virudhunagar 626-001, Tamilnadu, India

R. Anbarasan (✉)
Department of Chemical Engineering, Nano-Biotechnology Research Laboratory, National Taiwan University, Taipei 10617, Taiwan, ROC
e-mail: anbu_may3@yahoo.co.in

Introduction

For the past two decades, the materials' scientists and engineers have turned their research toward the synthesis of nano-sized materials particularly metal hydroxides for certain end-use applications. Due to their layer structure, complex forming behavior, multivalent nature, high thermal stability and ease of preparation, the metal hydroxides gain their own places. Recently, brucite-like structure compounds have provoked much intentions because of the versatile properties and excellent applications they showed in various science and engineering fields as catalyst, ion-exchanger, and so on. Such mega properties are mainly related to the structural features of such compounds. One of such a super potential compounds is nickel hydroxide ($Ni(OH)_2$). $Ni(OH)_2$ can be prepared in nano size. We can search for various methods available for the synthesis of nano-sized $Ni(OH)_2$ and physical and chemical characteristics of the same. The nano ribbon of $Ni(OH)_2$ was synthesized with the size of 5–25 nm and the thickness of 3–9 nm [1]. Dodecyl sulfate intercalated layered $Ni(OH)_2$ was synthesized and reported by Ida et al. [2]. Ramesh and Kamath [3] synthesized $Ni(OH)_2$ and characterized by FTIR and PXRD techniques. Nano-sized $Ni(OH)_2$ by solid-state reaction was reported in the literature [4]. Jiao et al. [5] and Dong et al. [6] published hydrothermal synthesis of nano rod and nano tubes of $Ni(OH)_2$. Taibi et al. [7] analyzed the basal spacing of layered $Ni(OH)_2$. The other research team also reported about the synthesis and characterization of nano-sized $Ni(OH)_2$ [8–17]. By thorough literature survey, we could not find any report regarding the synthesis and characterization of poly(vinyl alcohol) (PVA)/$Ni(OH)_2$ nano composite. Hence, our research team took such an effort for the first time. The selection of $Ni(OH)_2$ as a nano material candidature for this study is

due to the following reasons: $Ni(OH)_2$ is used as a cathodic electrodeposition material [18], forming complex with L-histidine [19], citric acid [20], pyrrole [21] and which can be easily synthesized through sonochemical method [22]. Hence, one can expect a complex formation with hydroxyl groups of PVA in aqueous medium to form PVA/$Ni(OH)_2$ nano composite. The PVA–metal salt complexes can be used as solid electrolytes in different energy conversion devices such as batteries/fuel cells, photo-electrochemical solar cells, electrochemical solar cells, and so on [23]. This is the key idea of this study. In this communication, we present the results on the effect of nano-sized $Ni(OH)_2$ on the structural and thermal properties of PVA as a novel way of approach.

Experimental

Materials

Aniline (ANI, AR, Merck, India) was purified by distillation before use. PVA (SD Fine Chemicals, AR, India) with the molecular weight of 1,25,000 (85% hydrolyzed) was used as received. Nickel sulfate (Reachem, AR, India) and sodium hydroxide (AR, Reachem) were purchased and used without further purifications. Doubly-distilled (DD) water was used for solution preparation purpose.

Synthesis of nano-sized $Ni(OH)_2$

2.808 g of nickel sulfate and 0.40 g of sodium hydroxide were taken in a 500-mL round-bottom flask charged with various concentrations of ANI in 200 mL DD water. The contents were stirred vigorously at 85 °C for 48 h. The reaction mixture was agitated continuously for another 48 h. The contents were filtered (the precipitate obtained was $Ni(OH)_2$ and dried at 110 °C for 6 h) through G4 sintered crucible. Thus, obtained nano crystalline $Ni(OH)_2$ powder was weighed and stored in a zipper bag.

Synthesis of PVA/$Ni(OH)_2$ nanocomposite

1 g of PVA was dissolved in 100 mL of DD water in a 250-mL round-bottle flask at 85 °C for 2 h. After the complete dissolution of PVA in water, 5 wt% nano-sized $Ni(OH)_2$ was added in a slow manner under vigorous stirring with nitrogen purging. After 3 h of vigorous stirring, the contents were poured onto a polyimide film and drying at 60 °C for 6 h. Thus, obtained PVA/$Ni(OH)_2$ nanocomposite film was subjected to various analytical characterizations.

Characterization

FTIR spectra of the samples were recorded by using FTIR-8400 S (Shimadzu, Japan) model instrument via KBr pelletization method. The peak area was determined after proper baseline correction. The relative intensity (RI) was measured as follows:

$$\text{RI of carbonyl peak} = \text{RI}_{[\text{C=O/CH}]} = A_{1733}/A_{844} \quad (1)$$

$$\text{RI of terminal double bond} = \text{RI}_{[\text{C=C/CH}]\text{TD}} = A_{1578}/A_{844} \quad (2)$$

$$\text{RI of middle double bond} = \text{RI}_{[\text{C=C/CH}]\text{MD}} = A_{1661}/A_{844} \quad (3)$$

where A indicates the corrected area of the peak, TD is terminal double bond, and MD is middle double bond. A double beam UV–Vis spectrophotometer (Hitachi 3010 UV-visible spectrophotometer, Japan) was employed for the UV–Vis spectral analysis of samples. The photoluminescence (PL) was carried out by an ElicoT spectrometer with the excited wavelength of 326 nm. TGA and differential scanning calorimetry (DSC) were carried out by using STA 409 (TA instrument, Japan) with the simultaneous TGA and DSC analysis system at the heating rate of 10 °C/min under air and nitrogen atmosphere, respectively. The morphology and the phase identification of the products were characterized by field-emission scanning electron microscopy (FESEM, JSM 6300, JEOL, Japan) (at 25 kV for SEM imaging), and X-ray diffraction (XRD, XS08, BRUKER, USA) was recorded with an advanced instrument and scanning from the 2θ value of 2 to 60° at a scanning rate of 2°/min. Furthermore, the size of $Ni(OH)_2$ was determined by high-resolution transmission electron microscopy (HRTEM, TEM 3010, JEOL, Japan) instrument.

Results and discussion

FTIR spectroscopy

Figure 1a showed the FTIR spectrum of pristine $Ni(OH)_2$. The OH stretching is appeared around 3500 cm^{-1} as a broad peak. The symmetric and anti-symmetric stretching of carbonate anion present in the interlayer space of $Ni(OH)_2$ is exhibited at 1630 and 1381 cm^{-1} respectively. The M–O stretching is shown at 627 cm^{-1}. Appearance of these peaks confirmed the chemical structure of pristine $Ni(OH)_2$. Figure 1b–f indicated the FTIR spectra of ANI-mediated synthesis of $Ni(OH)_2$. Here also one can observe the same peaks as mentioned above. In addition, appearance of one sharp peak at 3655 cm^{-1} confirmed the N–H

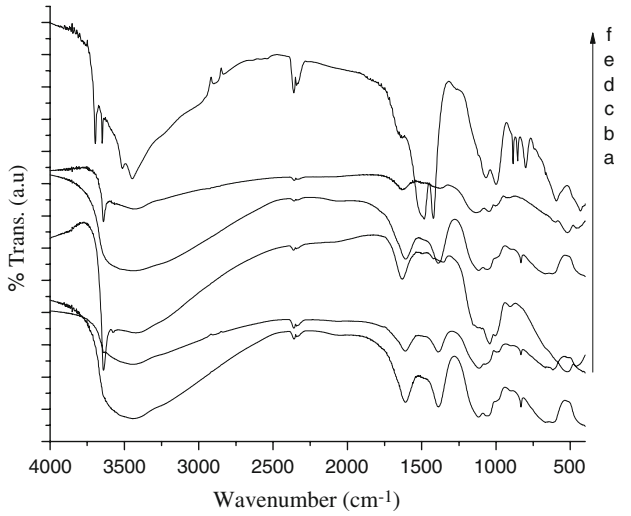

Fig. 1 FTIR spectrum of (*a*) pristine $Ni(OH)_2$, (*b*) $Ni(OH)_2$ + 1 wt% ANI, (*c*) $Ni(OH)_2$ + 3 wt% ANI, (*d*) $Ni(OH)_2$ + 5 wt% ANI, (*e*) $Ni(OH)_2$ + 7 wt% ANI, (*f*) $Ni(OH)_2$ + 9 wt% ANI

stretching vibration of ANI. This confirmed the intercalation of ANI into the basal spacing of layered $Ni(OH)_2$. Peak due to oxidized forms of ANI is not observed. This exhibited the poor intercalating nature of ANI into the basal spacing of $Ni(OH)_2$. Illia et al. [8] presented the FTIR spectrum similar to this study.

UV–Vis spectroscopy

Figure 2a indicated the UV–Vis spectrum of pristine $Ni(OH)_2$. A hump at 210 nm confirmed the presence of Ni^{2+} ions. Figure 2b, c indicated the 1 and 5 wt% ANI-mediated synthesis of $Ni(OH)_2$, respectively. A small peak around 370 nm indicated the presence of oxidized forms of ANI, present in the basal spacing of $Ni(OH)_2$. There is no red shifting of Ni^{2+} ion peak due to intercalation of ANI.

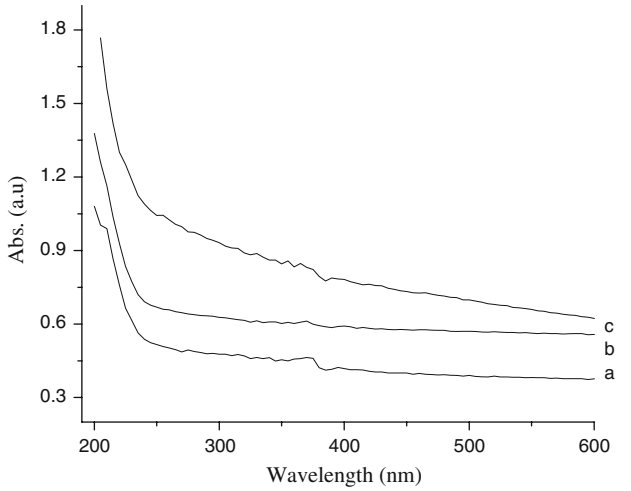

Fig. 2 UV–Vis spectrum of (*a*) pristine $Ni(OH)_2$, (*b*) $Ni(OH)_2$ + 1 wt% of ANI, (*c*) $Ni(OH)_2$ + 5 wt% of ANI

TGA profile

Thermal stability of pristine $Ni(OH)_2$ was analyzed by recording TGA under air atmosphere at a heating rate of 10 °C/min. As shown in Fig. 3a, the thermogram showed a two-step degradation process. The first minor weight loss step up to 250 °C is due to the removal of moisture, physisorbed, and chemisorbed water molecules. The second major weight loss step up to 420 °C is responsible for the de-hydroxylation of $Ni(OH)_2$ leads to the removal of water molecules. Above 750 °C, it showed 66 wt% residue remained. Figure 3b indicated the 5 wt% ANI-mediated synthesis of $Ni(OH)_2$. This system also exhibited the same pattern of degradation process. However, the de-hydroxylation temperature is slightly increased. The increase in temperature around 275 °C is due to two reasons. The first reason gives an assurance of intercalation of ANI moieties in to the basal spacing of $Ni(OH)_2$. The second reason is due to the formation of complex between amino group of ANI and Ni^{2+} ions. Complex forming behavior of nickel ion is well discussed in the literature [19–21] and hence further discussion on this topic is not required here. Above 750 °C, it showed 68 wt% residue remained. Dong et al. [6] synthesized nano $Ni(OH)_2$ and they studied the thermal stability of the same. Both α and β forms of $Ni(OH)_2$ decomposed even before 350 °C. Various sulfonate and nitrate-intercalated $Ni(OH)_2$ also showed complete degradation before 300 °C [7]. On comparison with other's results, our system showed the maximum degradation at 400 °C in the presence and absence of dispersant. This proved that $Ni(OH)_2$ synthesized by co-precipitation method exhibited better thermal stability.

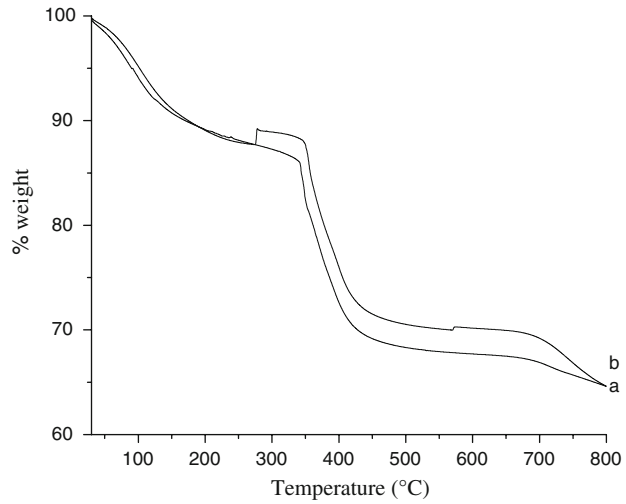

Fig. 3 TGA of (*a*) $Ni(OH)_2$, (*b*) $Ni(OH)_2$ + 5 wt% ANI

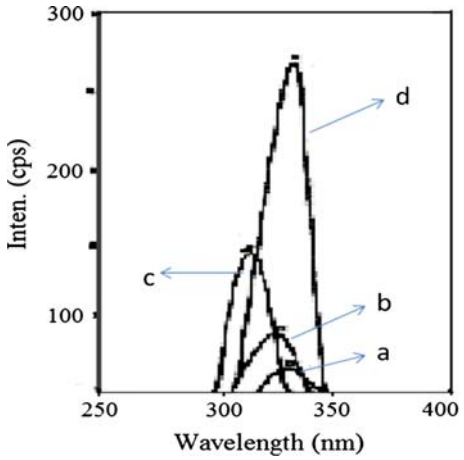

Fig. 4 PL of (*a*) pristine $Ni(OH)_2$, (*b*) $Ni(OH)_2$ + 5 wt% ANI, (*c*) pure PVA, (*d*) $Ni(OH)_2$ + 5 wt% ANI + PVA

Photoluminescence

$Ni(OH)_2$ showed a sharp peak at a wavelength of 338 nm with the intensity of 1.803 mV in Fig. 4a. Figure 4b shows the PL of $Ni(OH)_2$ synthesized in the presence of 5 wt% of ANI as a dispersing agent. In the presence of ANI, there was a blue shift in the wavelength of $Ni(OH)_2$, i.e., 327 nm, but its intensity rose to 38.209 mV. The sudden increase in intensity is due to the presence of chromophoric amino group (ANI) in the interlayer space of $Ni(OH)_2$, i.e., intercalation reaction of ANI into the basal spacing of the layered $Ni(OH)_2$. PL study was carried out for pure PVA (Fig. 4c). The sharp peak was appeared at a wavelength of 321 nm with the maximum intensity at 6.74 mV. This value is compared with PL value of the hybrid, i.e., $Ni(OH)_2$ +5 wt% of ANI. The PL value for the PVA + 5 wt% of ANI-intercalated $Ni(OH)_2$ is shown in Fig. 4d. Here, the intensity value was found to be 16 mV. In PVA–$Ni(OH)_2$–5 wt% ANI system, the wavelength was blue shifted to 301 nm. The shift in the wavelength of the nanocomposites clearly explained the existence of interaction between PVA and $Ni(OH)_2$ hybrid. All the samples were excited at 260 nm.

Scanning electron microscopy

The morphology of pristine $Ni(OH)_2$ was fragile, in spite of compact appearance and clusters of a large amount of nanometric particles (Fig. 5a). Figure 5b revealed the morphology of 1 wt% of ANI-intercalated $Ni(OH)_2$. Here, nano rod-like morphology was observed. This inferred that at lower concentration of dispersing agent like ANI, the morphology of $Ni(OH)_2$ was completely affected; however, it activated the formation of $Ni(OH)_2$. Figure 5c showed 5 wt% of ANI-intercalated $Ni(OH)_2$ with different morphology. The micrograph showed more number of nano particles but with agglomerated structure. Even though the FESEM images are qualitative one, this infers

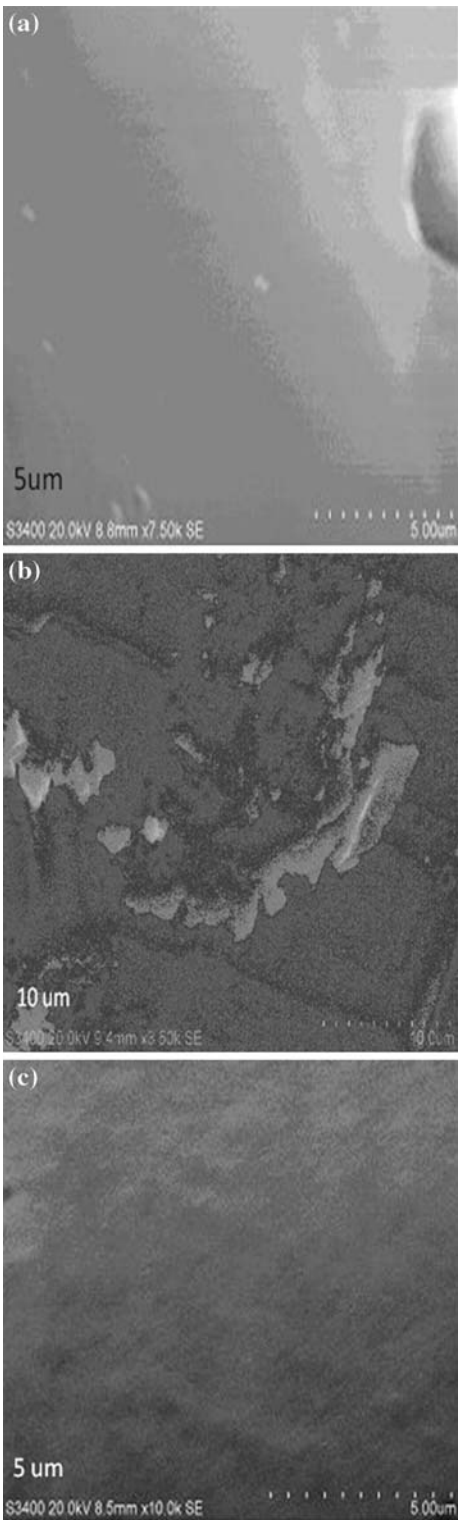

Fig. 5 SEM image of **a** pristine $Ni(OH)_2$, **b** $Ni(OH)_2$–5 wt% ANI, **c** $Ni(OH)_2$ + 5 wt% ANI

that the synthesis of $Ni(OH)_2$ in the presence of higher % weight of ANI leads to the agglomer structure and hence it is not suitable for the synthesis of nano particles of $Ni(OH)_2$. Because the role of increment in ANI can be analyzed through seeing the FESEM images and which exhibits the different morphology with increase in % weight of $Ni(OH)_2$. Ni et al. [9] published the FESEM of β-$Ni(OH)_2$. In which, the author reported the flower-like morphology. $Ni(OH)_2$ synthesized via urea decomposition showed the surface morphology of spherical agglomerate sheet like nanometer scale crystallites [11]. Our results are in agreement with Ref. [11].

High-resolution transmission electron microscopy

Figure 6 indicated the HRTEM of pristine $Ni(OH)_2$. Figure 6a showed the layered structure of $Ni(OH)_2$. Figure 6b showed the agglomerated structure of $Ni(OH)_2$ with different morphological appearances. The selected-area electron diffraction (SAED, Fig. 6c) indicated the bright spots in a circular pathway. This confirmed the crystalline nature of $Ni(OH)_2$. Figure 7 indicated the topography of 5 wt% ANI-mediated synthesis of $Ni(OH)_2$. Here also one can observe the agglomerated structure. However, the agglomeration (Fig. 7a) took place in a linear manner and not like a bulk agglomeration in pristine $Ni(OH)_2$. The photographs indicated the nano tubes-like morphology with 80 nm diameter (Fig. 7b). The length is 2–3 μm. The SAED (Fig. 7c) confirmed the amorphous nature of 5 wt% of ANI-mediated synthesis of $Ni(OH)_2$. HRTEM suggested that the utilization of higher % weight of dispersing agent affected the morphology as well as the crystalline nature of $Ni(OH)_2$. Boyer et al. [12] reported the nano platelet-shape morphology for $Ni(OH)_2$. Yang et al. [13] reported the FESEM and TEM images of $Ni(OH)_2$. Our HRTEM results are entirely different from the above-mentioned references. This is due to the presence of ANI, the dispersant present in the basal spacing of $Ni(OH)_2$.

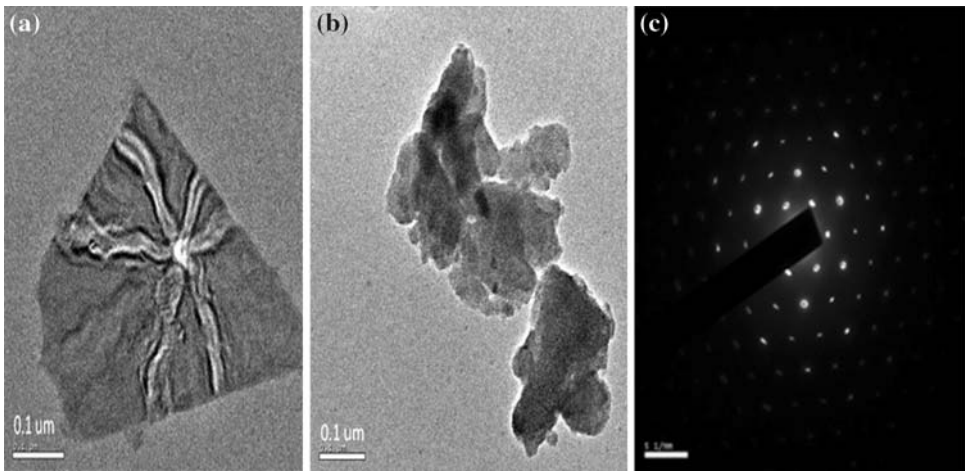

Fig. 6 HRTEM of pristine $Ni(OH)_2$

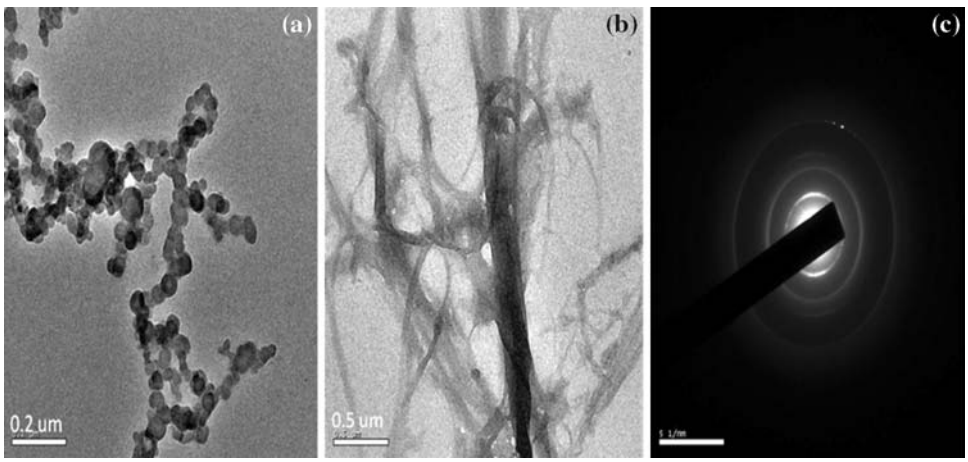

Fig. 7 HRTEM of $Ni(OH)_2$–5 wt% ANI

Fourier transform infrared spectroscopy

Figure 8 represented the FTIR spectra of PVA loaded with $Ni(OH)_2$ at different % weight. The important peaks are characterized below. A broad peak around 3500 cm^{-1} indicated the OH stretching vibration. The C–H stretching vibration was observed at 2930 cm^{-1}. A peak at 1723 cm^{-1} accounted the carbonyl stretching vibration. The C=C stretching have been observed at 1661 (terminal double bond) and 1577 cm^{-1} (middle double bond). The C–H out of plane bending vibration can be seen at 844 cm^{-1}. The metal–oxide stretching was observed at 638 cm^{-1}. The FTIR spectrum showed similar peaks in all % weight loadings of nano material, the only different is the increase in RI of carbonyl and alkene groups. By using FTIR software, one can quantitatively find out the difference in PVA structure by the way of measuring the carbonyl group formation and olefin formation. The added nano-sized $Ni(OH)_2$ altered the structure of PVA via surface catalytic effect. The PVA + $Ni(OH)_2$ nanocomposite was prepared in aqueous medium with different % weight of $Ni(OH)_2$. During the course of preparation of $Ni(OH)_2$ nanocomposite in aqueous medium, there is a chance for the thermolytic oxidation reaction, i.e., olefin formation and chain scission reactions (Fig. 9). In this study, we have noted the effect of $Ni(OH)_2$ on PVA structure. Here, we followed mainly two types of reactions during the nanocomposite formation: (i) appearance of carbonyl stretching at 1730 cm^{-1} due to the conversion of secondary alcoholic group into a ketone group; (ii) due to thermal and hydrolytic oxidation reaction there is a chance for the formation of olefin bonds, i.e., formation of C=C. The double bond could be formed at the end of the polymer chain end

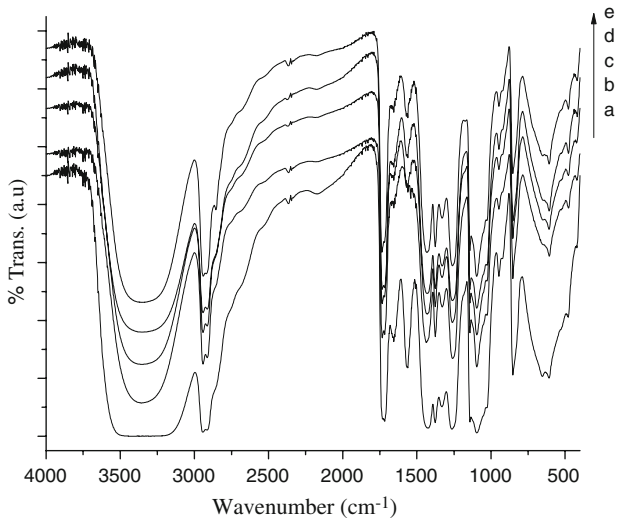

Fig. 8 FTIR spectrum of PVA loaded with $Ni(OH)_2$ at (*a*) 1 wt%, (*b*) 3 wt%, (*c*) 5 wt%, (*d*) 7 wt%, and (*e*) 9 wt%

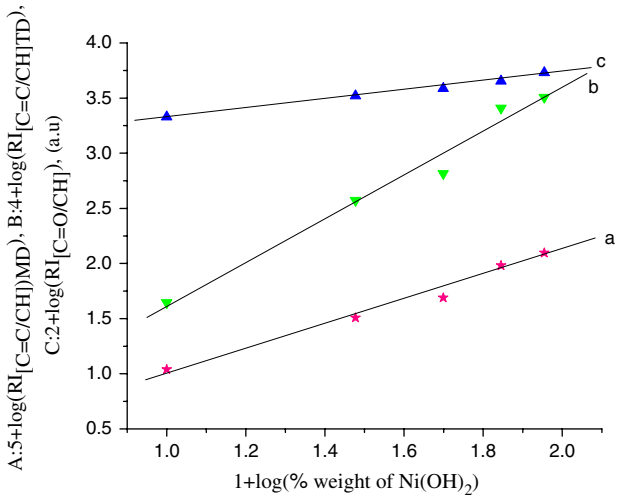

Fig. 9 Effect of % weight of $Ni(OH)_2$ on (*a*) $RI_{[C=C/CH]MD}$, (*b*) $RI_{[C=C/CH]TD}$, (*c*) $RI_{[C=O/CH]}$. Weight of PVA = 1.0 g, time = 3 h, temperature = 80 °C

(1630 cm^{-1}) or at the middle of the polymer chain. It was found that while increased the % weight of nano material, the RI of carbonyl formation and C=C formation was also increased. By using FTIR software, the change in relative intensity of the carbonyl and C=C was quantitatively calculated and the order of formation reaction was determined from the same. The data points well agreed with the fitted lines through R^2 value method. Currently, Anbarasan and research team explained the quantitative application of FTIR spectroscopy in the structural investigation of electrically conducting polymer [24].

The C=C formation was quantitatively determined by using the FTIR software. The plot of log (% weight of $Ni(OH)_2$) versus log ($RI_{[C=C/CH]TD}$) (Fig. 9a) followed the 0.89 order of reaction and log (% weight of $Ni(OH)_2$) versus log ($RI_{[C=C/CH]MD}$) (Fig. 9b) followed the 0.616 order of reaction with respect to % weight of nano-sized $Ni(OH)_2$. The increase in RI of [C=C/CH] indicates that there is a decrease in molecular weight through the removal of hydrogen atom from PVA backbone due to the surface catalytic effect of nano-sized $Ni(OH)_2$. The reduction in molecular weight of PVA is under investigation in our lab through GPC measurements. While increasing the % weight of $Ni(OH)_2$ from 1 to 9 wt%, the carbonyl group formation is increased linearly. In order to find out the order of carbonyl group formation reactions, the plot of log (% weight of $Ni(OH)_2$) versus log ($RI_{[C=O/CH]}$) (Fig. 9c) was drawn and the plot was found to be a straight line with the slope of 0.99. This indicated the 1.0 order of carbonyl formation reaction with respect to (% weight of $Ni(OH)_2$). These results indicated that the added nano-sized $Ni(OH)_2$ accelerated the formation of double bonds, particularly terminal double bonds via chain scission process, which led to the

reduction in molecular weight of PVA. The decrease in molecular weight is under investigation in our lab through GPC measurements. At this moment, the increase in RI of [C=C/CH] confirms the decrease in molecular weight of PVA. For the first time, we are reporting here about the amount of double bond formation during the PVA–$Ni(OH)_2$ nano composite formation quantitatively by using FTIR spectra. Recently, our research team has communicated the FTIR-based kinetic results on the RI of carbonyl formation and alkenes formation [25].

UV–Vis spectroscopy

UV–Vis spectrum of pristine $Ni(OH)_2$ and nano composite with PVA in different % weight loading is shown in Fig. 10. $Ni(OH)_2$ after making composite with PVA, its original absorbance value is disappeared. This is due to the complex formation nature of $Ni(OH)_2$ with hydroxyl group of PVA matrix. Moreover, identification of Ni^{2+} ion is very difficult at lower % weight loading of $Ni(OH)_2$ in PVA matrix, whereas at higher % weight loading, due to agglomeration process the added nano material formed a cluster with bundle-like structure without any physical or chemical interaction with PVA matrix. As a result, the bundled nano materials were precipitated from the reaction medium. This inferred that at very low as well as at very high % loading of Ni^{2+} ions it was very difficult to identify the same in the UV–Vis spectrum.

TGA history

Figure 11a indicated the TGA of 1 wt% $Ni(OH)_2$-loaded PVA nanocomposite (Table 1). The thermogram showed a three-step degradation process. The first minor weight loss

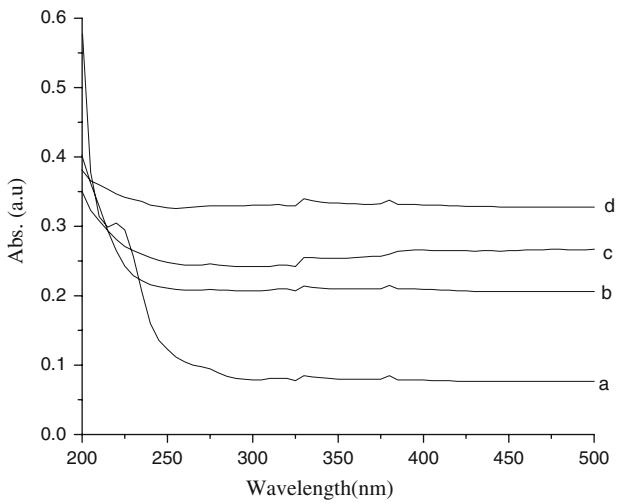

Fig. 10 UV–Vis spectrum of (*a*) pristine $Ni(OH)_2$, (*b*) PVA–1 wt% $Ni(OH)_2$, (*c*) PVA–3 wt% $Ni(OH)_2$, (*d*) PVA–5 wt% $Ni(OH)_2$

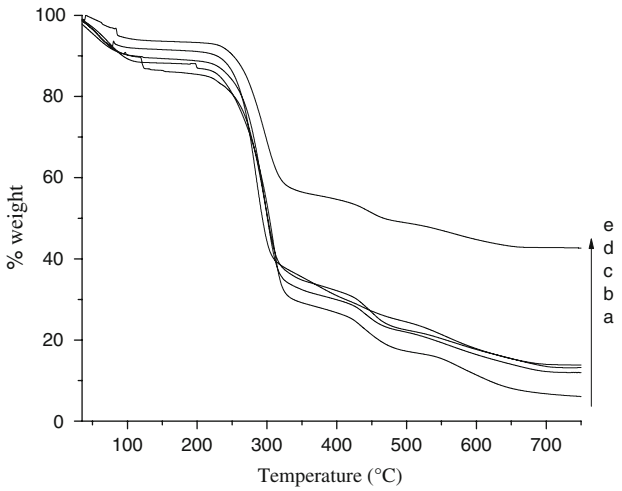

Fig. 11 TGA of PVA loaded with $Ni(OH)_2$ at (*a*) 1 wt%, (*b*) 3 wt%, (*c*) 5 wt%, (*d*) 7 wt%, (*e*) 9 wt%

step up to 200 °C accounted the removal of moisture, physisorbed, and chemisorbed water molecules. While increasing the temperature further that led to the breaking of intermolecular hydrogen bonding with simultaneous degradation of PVA backbone. Above 400 °C, it led to the degradation of intercalated PVA chains. Above 700 °C, the % weight residue increased with the increment of % weight of $Ni(OH)_2$. But the increment in % weight residue is low, because of intermolecular condensation between $Ni(OH)_2$ with the removal of water molecules at higher temperature. But at higher % weight loading, particularly at 9 wt% of $Ni(OH)_2$, due to agglomeration process the increment in % weight residue is suddenly increased. Figure 12b–e represented the TGA of 3, 5, 7, and 9 wt% $Ni(OH)_2$-loaded PVA chains, respectively. It is noteworthy that while increased the % weight of $Ni(OH)_2$, the initial degradation temperature (T_{id}) of PVA was also increased. This explained the interaction between PVA and loaded nano-sized $Ni(OH)_2$.

Differential scanning calorimetry

Differential scanning calorimetry of PVA loaded with different % weight of $Ni(OH)_2$ was shown in Fig. 12. The de-watering temperature (T_{dw}) of PVA/$Ni(OH)_2$ nanocomposite was appeared at 125 °C. The T_α was appeared at 194 °C. The T_m was appeared at 280 °C. While increasing the % weight of $Ni(OH)_2$, there was slight increase in the T_{dw} and T_α. However, there was an abnormal increase in T_m with respect to the increase in % weight of $Ni(OH)_2$ was observed. The 1 wt% $Ni(OH)_2$-loaded PVA showed the T_m value of 290 °C, whereas the 5 wt% $Ni(OH)_2$-loaded PVA showed the same at 323.1° C. This is due to the following reasons: (i) presence of hydrogen bonding between PVA and $Ni(OH)_2$, (ii) hydrolytic oxidation reaction of PVA

Table 1 TGA of PVA loaded with different % weight of $Ni(OH)_2$

System	% weight at 200 °C	% weight at 300 °C	% weight at 400 °C	% weight at 500 °C	% weight above 650 °C
PVA–1 wt% $Ni(OH)_2$	87.6	54.3	26.6	17.1	6.5
PVA–3 wt% $Ni(OH)_2$	89.0	52.1	30.5	22.1	12.2
PVA–5 wt% $Ni(OH)_2$	85.5	52.6	31.9	23.2	13.5
PVA–7 wt% $Ni(OH)_2$	91.1	53.3	32.8	24.4	14.3
PVA–9 wt% $Ni(OH)_2$	93.6	69.2	54.8	48.8	42.5

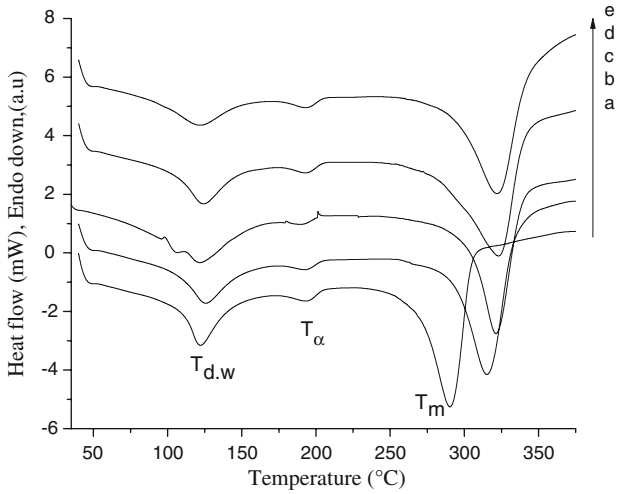

Fig. 12 DSC of PVA loaded with $Ni(OH)_2$ at (*a*) 1 wt%, (*b*) 3 wt%, (*c*) 5 wt%, (*d*) 7 wt%, (*e*) 9 wt%

(hydroxyl group of PVA is converted into keto group), (iii) reduction in molecular weight due to thermolytic oxidation could be compensated by interaction with $Ni(OH)_2$, (iv) complex formation between the hydroxyl group of PVA and $Ni(OH)_2$.

Conclusions

In summary, nano-sized $Ni(OH)_2$ prepared by co-precipitation method with the help of ANI as a self-assembly yielded favorable results. FTIR spectrum confirmed the presence of metal hydroxide stretching in the $Ni(OH)_2$. TGA showed the improved thermal stability above 750 °C. The 5 wt% ANI-intercalated $Ni(OH)_2$ showed a nano tube-like morphology with the size of 80 nm, whereas the pristine $Ni(OH)_2$ showed nano sheet-like morphology. SEM inferred that pristine $Ni(OH)_2$ showed nano rod-like morphology, whereas 5 wt% of ANI-intercalated $Ni(OH)_2$ showed the agglomerated morphology. UV–Vis spectrum confirmed the presence of Ni^{2+} ion at 210 nm and the presence of amino group the hybrid system showed a sharp peak at 326 nm and the intensity of which increased along with the increase in % weight of ANI. PL inferred that ANI-intercalated $Ni(OH)_2$ showed a higher intensity value than the pristine and nanocomposite systems. Using FTIR software, the order of formation of middle double bond (followed a 0.50 order of reaction) and terminal double bond (obeyed 1.0 order of reaction) and carbonyl group formation (accepted the 1.0 order of reaction) with respect to (% weight of $Ni(OH)_2$) was determined. TGA of $Ni(OH)_2$-loaded PVA showed slight increase in T_{id}. DSC exhibited the increase in T_m value of PVA–$Ni(OH)_2$ nano composite systems.

References

1. Yang D, Wang R, He M, Zhang J, Liu Z (2005) J Phys Chem B 109:7654. doi:10.1021/jp050083b
2. Ida S, Shiga D, Koinuma M, Matsumoto Y (2008) J Am Chem Soc 130:14038. doi:10.1021/ja804397n
3. Ramesh TN, Kamath PV (2006) J Power Sources 156:655. doi:10.1016/jpowsour.2005.05.050
4. Liu X, Yu L (2004) Mater Lett 58:1327. doi:10.1016/j.matlet.2003.09.054
5. Jiao QZ, Tian ZL, Zhao Y (2007) J Nanopart Res 9:519. doi:10.1007/s11051-006-9088-3
6. Dong L, Chu Y, Sun W (2008) Chem Eur J 14:5064. doi:10.1002/chem.200701627
7. Taibi M, Ammar S, Jouini N, Drillon M (2002) J Mater Chem 12:3238. doi:10.1039/b204087e
8. Illia GS, Jobbagy M, Regazzoni AE, Blesa MA (1999) Chem Mater 11:3140. doi:10.1021/cm9902220
9. Ni X, Zhao Q, Cheng J, Zhang D (2005) Chem Lett 34:1408. doi:10.1246/cl.2005.1408
10. Liu X, Qiu G, Wang Z, Li X (2005) Nanotechnology 16:1400. doi:10.88/0957-4484/16/8/071
11. Akinc M, Jongen N, Lemaitre J, Hofman H (1988) J Eur Ceram Soc 18:1559
12. Boyer JM, Repetti B, Garrigos R (2004) J Metastable Nanocryst Mater 22:1
13. Yang LX, Zhu YJ, Tong H, Zhang L (2007) J Solid State Chem 180:2095. doi:10.1016/j.jssc.2007.05.009
14. Wu XF, Chen YF, Li QY (2007) Solid State Phenom 121–123:187
15. Wang D, Song C, Hu Z, Fu X (2005) J Phys Chem B 109:1125. doi:10.1021/jp0467970
16. Bernard MC, Cortes R, Keddam M, Senyarich S (1996) J Power Sources 63:247
17. Watanabe K, Kikuoka T, Kumagai N (1995) J Appl Electrochem 25:219
18. Zhitominsky I (2004) Mater Lett 58:420. doi:10.1016/S0167-577x(03)00516-0
19. Kostromina NA, Tikhonov VP (1980) Khimiya 16:511

20. Hedwig GR, Liddle JR, Reeves RD (1980) Aust J Chem 33:1685
21. Stunzi H, Anderegg G (1976) Helv Chim Acta 59:1621
22. Jeevanandam P, Gedankan A (2001) Nano Lett 1:263
23. Smitha B, Sridhar S, Khan AA (2005) J Membr Sci 259:10. doi: 10.1016/j.memsci.2005.01.035
24. Rathika S, Duraimurugan K, Dhanalakshmi V, Anbarasan R (2009) J Mater Sci. doi:10.1007/s10853-009-3478-8
25. Fathima Parveen M, Umapathy S, Anbarasan R Mater Chem Phys (submitted)